UNIVERSITY OF AMSTERDAM

UvA-DARE (Digital Academic Repository)

A suit of armor around ADAMTS13

Exploring paths towards resistance against autoantibodies of immune TTP patients

Gomes Graça, N.A.

Publication date
2021

Link to publication

Citation for published version (APA):
Gomes Graça, N. A. (2021). *A suit of armor around ADAMTS13: Exploring paths towards resistance against autoantibodies of immune TTP patients*. [Thesis, externally prepared, Universiteit van Amsterdam].

General rights
It is not permitted to download or to forward/distribute the text or part of it without the consent of the author(s) and/or copyright holder(s), other than for strictly personal, individual use, unless the work is under an open content license (like Creative Commons).

Disclaimer/Complaints regulations
If you believe that digital publication of certain material infringes any of your rights or (privacy) interests, please let the Library know, stating your reasons. In case of a legitimate complaint, the Library will make the material inaccessible and/or remove it from the website. Please Ask the Library: https://uba.uva.nl/en/contact, or a letter to: Library of the University of Amsterdam, Secretariat, P.O. Box 19185, 1000 GD Amsterdam, The Netherlands. You will be contacted as soon as possible.

UvA-DARE is a service provided by the library of the University of Amsterdam (https://dare.uva.nl)

Download date:18 Nov 2026

5

Chapter 5

N-glycan mediated shielding of ADAMTS13 prevents binding of pathogenic autoantibodies in immune-mediated TTP

Bogac Ercig*, **Nuno A. G. Graça***, Kadri Kangro*, Kanin Wichapong, Johana Hrdinová, Paul Kaijen, Floris P.J. van Alphen, Maartje van den Biggelaar, Karen Vanhoorelbeke, Agnès Veyradier, Paul Coppo, Chris Reutelingsperger, Gerry A.F. Nicolaes, Andres Männik and Jan Voorberg

These authors contributed equally

Blood 2021; (First Edition, 5th February 2021); doi: 10.1182/blood.2020007972

Abstract

Immune-mediated thrombotic thrombocytopenic purpura (iTTP) is an autoimmune disorder caused by the development of autoantibodies targeting different domains of ADAMTS13. Profiling studies have shown that residues R568, F592, R660, Y661 and Y665 within exosite-3 of the spacer domain provide an immunodominant region of ADAMTS13 for pathogenic autoantibodies that develop in patients with iTTP. Modification of these 5 core residues with the goal of reducing auto-antibody binding revealed a significant trade-off between autoantibody resistance and proteolytic activity. Here, we employed structural bioinformatics to identify a larger epitope landscape on the ADAMTS13 spacer domain. Models of spacer–antibody complexes predicted that residues R568, L591, F592, K608, M609, R636, L637, R639, R660, Y661, Y665 and L668 contribute to an expanded epitope within the spacer domain. Based on bioinformatics guided predictions we designed a panel of N-glycan insertions in this expanded epitope to reduce the binding of spacer domain autoantibodies. One N-glycan variant (NGLY3-ADAMTS13 containing a K608N substitution) showed strongly reduced reactivity with TTP patient sera (28%) as compared to WT-ADAMTS13 (100%). Insertion of an N-glycan at amino acid position 608 did not interfere with processing of VWF positioning the resulting NGLY3-ADAMTS13 variant as a potential novel therapeutic option for treatment of iTTP.

Introduction

Immune-mediated thrombotic thrombocytopenic purpura (iTTP) is a rare life-threatening autoimmune disease.[1–3] In iTTP, the von Willebrand Factor (VWF) cleaving protease ADAMTS13 is targeted by autoantibodies[4] which leads to loss of its proteolytic activity[5] and/or enhanced clearance[6] of ADAMTS13. A major epitope (R568/F592/R660/Y661/Y665)[4,7–9] for autoantibodies is located in the spacer domain exosite-3 which also provides an interaction hub for VWF.[9,10] Early studies revealed that modification of exosite-3 resulted in impaired binding of autoantibodies.[4,7] Conservative amino acid substitutions within exosite-3 yielded a so-called Gain-of-Function (GoF) ADAMTS13 variant that conferred resistance to autoantibodies.[8] In contrast to these findings, quantitative assessment of autoantibody binding using an extensive panel of conservative, semi-conservative and non-conservative exosite-3 variants indicated that also non-conservative substitutions that included the GoF variant did not alleviate the binding of pathogenic autoantibodies.[10] Semi-conservative and non-conservative substitutions did result in a significant loss of autoantibody binding but also reduced proteolytic activity.[10] In the current study, we employed structural bioinformatics to explore a larger epitope landscape on the ADAMTS13 spacer domain. Newly generated autoantibody-spacer domain complex models were used to design novel variants capable of resisting patient autoantibody binding. We show that artificially inserted N-glycans prohibit binding of pathogenic autoantibodies while retaining normal levels of proteolytic activity.

Study design

3D structural models of Fv (variable fragments) from patient-derived monoclonal anti-ADAMTS13 autoantibodies II-1 and I-9[5,11] were built (Figure 1A).[12,13] The possible complex formations between ADAMTS13 cysteine-rich/spacer domain crystal structure (Protein Data Bank ID: 3GHM)[14] and Fv models were generated by protein-protein docking (Figure 1B).[15] Each docking pose for the wild type (WT) antigen-autoantibody complex was also exploited to generate gain-of-function (GoF) ADAMTS13 mutations (R568K/F592Y/R660K/Y661F/Y665F)[8] which were subjected to simulate and investigate a loss of interactions between patient derived monoclonal antibodies and these classic exosite-3 epitope residues. As previously shown[8] and here, II-1 and I-9 can no longer bind to GoF-ADAMTS13. The WT and GoF complexes were used in molecular dynamics (MD) simulations (Figure 1C)[16] to determine the most likely binding pose for II-1 and I-9 by means of binding free energy (BFE) calculation,[17–19] ; the lowest BFE (highest affinity) for the WT-antigen-autoantibody complex (compared to the GoF-antigen-autoantibody complex; Figure 1D). The selected complexes for I-9

and II-1 were further investigated at a residue level on the spacer domain and a larger epitope landscape was predicted by our models. These predicted residues were mutated to an alanine. Alternatively, putative N-glycan attachment sequences were inserted in the loops where these residues are located (Supplementary Table 1). These variants were produced in CHO cells, quantified and the binding of each variant was measured against II-1, I-9 and a cohort of previously characterized iTTP patients' sera as previously described.[10] The activity level of each variant was also measured with a FRETS-VWF73[20] and VWF multimer assay.[10] The presence of N-glycans was experimentally determined by mass spectrometry (further details of the experimental procedures are available in the Supplementary Methods and Data).

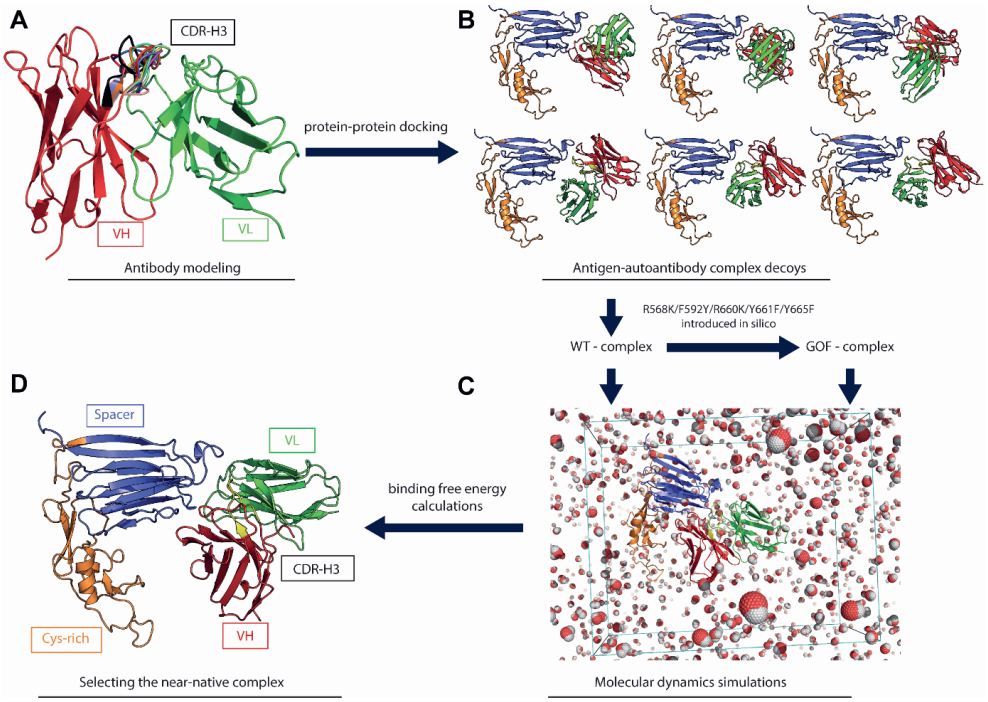

Figure 1 – Structural bioinformatics pipeline to build an antigen-autoantibody complex.

A. Antibody modeling of the II-1 and I-9 autoantibodies Fv fragments. Heavy chain (VH; shown in red) and light chain (VL; shown in green) built and orientated with each other. Complementary determining region 3 of VH (CDR-H3; shown in multiple colors) was grafted at different conformations to the Fv model. **B.** Docking results of ADAMTS13 antigen-autoantibody complex following the protein-protein docking step. **C.** Molecular dynamics simulations for each WT- and GoF-decoy model were run. **D.** A likely complex between ADAMTS13 antigen and autoantibody was selected by binding free energy calculations.

Results and Discussion

Models of ADAMTS13 spacer and II-1/I-9 autoantibody complexes predict a larger epitope landscape

The antigen-autoantibody complex models predicted an expansion of the previously determined epitope area in autoantibody binding. The model of the spacer–I-9 complex predicted that residues R568, L591, F592, K608, M609, R636, L637, R660, Y661, Y665 and L668 together form a larger epitope. The model of spacer–II-I complex predicted involvement of the same residues as well as R639. (Figure 2A; Supplementary Table 1). Unexpectedly, all of the novel single alanine variants (Figure 2A; depicted in yellow) were still capable of binding to patient-derived monoclonal antibodies II-1 and I-9 (Figure 2B), while the single alanine variants of classic epitope residues (Figure 2A; depicted in magenta) displayed a varying but much stronger reduction in binding. This may reflect to a lower contribution of these residues to autoantibody binding compared to several of the core classic R568/F592/R660/Y661/Y665 residues, despite the predicted interactions (Supplementary Table 1).

N-glycan variants of ADAMTS13 can resist against II-1 and I-9

Putative N-glycan motifs (Supplementary Table 1) were inserted as a complementary approach to cause a steric hindrance on the spacer epitope for autoantibodies. As shown in Figure 2B, variants NGLY1, NGLY5 and NGLY6 were able to resist against autoantibody II-1 and only NGLY1 and NGLY4 were partly resistant against I-9. NGLY2 and NGLY3 did not show any resistance against II-1 and I-9.

Variant NGLY3 can resist against autoantibody repertoires of TTP patients

All above-mentioned variants of ADAMTS13 were tested against a cohort of iTTP patients' sera (n=13). As previously shown,[10] single alanine mutations did not reduce binding against patient sera significantly (Figure 2C). Only F592A and K608A were able to cause a mild reduction to ~70% of WT-ADAMTS13 binding. In contrast, reduced median binding (up to 50-55%) of patients' autoantibodies to NGLY1, NGLY2, NGLY4 and NGLY6 was observed. Binding of patient derived autoantibodies to NGLY5 was only mildly affected. Interestingly, variant NGLY3 showed the lowest median binding against the patients sera (28%) suggesting that insertion of an N-glycan at amino acid position 608 efficiently shields binding of autoantibodies to the spacer domain in 10 of 13 patients (below 50%). In the rest of the patients, 2 out of 3 had C-terminal autoantibodies (TTP-079 and TTP-085) (Figure 2C).

Proteolytic activity of ADAMTS13 variants.

Subsequently, we addressed whether the ADAMTS13 variants described above were

still capable of cleaving VWF. Among all single alanine variants, F592A and R660A were the only variants which resulted in reduced activity relative to WT-ADAMTS13 in FRETS-VWF73 (Figure 2D). Other exosite-3 variants (R568A and Y661A) retained an identical activity to WT-ADAMTS13. Variant Y665A, together with all other expanded-epitope single alanine mutant variants (L591A, K608A, M609A, R636A, L637A and L668A) resulted in higher activity than WT-ADAMTS13 in FRETS-VWF73. The activity of single alanine ADAMTS13 variants tested against recombinant VWF multimers in a static assay is in concordance with results obtained using FRETS-VWF73 (Supplementary Figure 1).

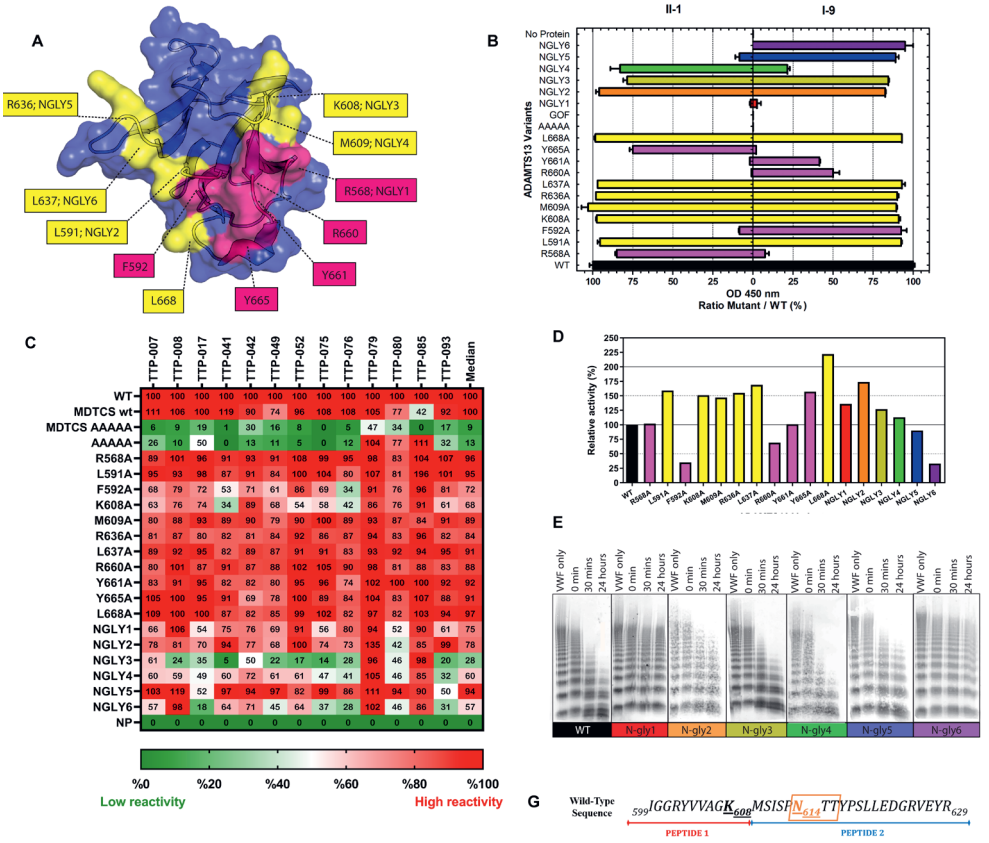

Figure 2 –

A. ADAMTS13 epitope expansion based on modeling. **B.** Reactivity of ADAMTS13 variants against II-1 and I-9 monoclonal autoantibodies. **C.** Reactivity of ADAMTS13 variants against TTP patient sera in heat map format. Numbers represent relative binding compared to wild type (in percentage; 100% is red, 50% is white, and 0% is green). **D.** Relative activity of ADAMTS13 variants in FRETS-VWF73 assay (WT-ADAMTS13 is 100%). **E.** Activity of NGLY-ADAMTS13 variants in VWF multimer assay. **F.** Relative activity of ADAMTS13 variants measured with FRETS-VWF73 in the presence of TTP patient sera (WT-

ADAMTS13 is 100%; all values compared to WT-ADAMTS13 without any patient antibodies). **G.** Mass spectrometry reveals presence of an N-glycan at amino acid position 608 in NGLY3 (K608N). The presence of glycan at this position is derived from the detection of a K608N containing deamidated peptide of NGLY3 upon treatment with PNGaseF (further details see Supplementary Information).

With FRETS-VWF73, variants NGLY1-5 displayed similar or higher activity when compared to WT-ADAMTS13. Variant NGLY6 was significantly less active than WT-ADAMTS13 (Figure 2D). The ability of NGLY1 and NGLY6 to process VWF multimers was strongly reduced (Figure 2E). Slightly reduced levels of VWF multimer processing were observed for NGLY2 and NGLY5 whereas NGLY3 and NGLY4 were similarly active as WT-ADAMTS13 (Figure 2E). NGLY3 was subsequently tested for activity together with an excess of patient autoantibodies in a FRETS-VWF73 assay.[10] In accordance with its reduced binding to patient autoantibodies, NGLY3 retained its ability to process FRETS-VWF73 in the presence of patient sera (Figure 2F). The presence of an additional N-glycan on NGLY3-ADAMTS13 was confirmed in mass spectrometry by the detection of K608N deamidation upon deglycosylation (Figure 2G). The N-glycan prevents the binding of pathogenic antibodies while it does not hamper proteolytic activity. Based on these properties we suggest that the NGLY3-ADAMTS13 variant may potentially be used to rapidly restore the VWF-ADAMTS13 axis in patients suffering from acute iTTP.

Authorship Contributions

B.E., N.A.G.G., G.N. and J.V. designed the study. K.K. and A.M. constructed and expressed ADAMTS13 variants. B.E., N.A.G.G. and K.K. performed experiments. B.E., J.H. G.A.F.N., C.P.R and K.W. performed or supervised the computational modeling. K.V. provided antibodies 3H9, biotinylated 17G2 and 19H4 for quantitation of recombinant ADAMTS13. A.V. and P.C. provided patient samples. F.P.J.v.A. and M.v.d.B. performed mass spectrometry. B.E., N.A.G.G. and J.V. wrote the manuscript. All authors critically revised the manuscript before submission.

Acknowledgements

This project has received funding from the European Union's Horizon 2020 research and innovation programme under the Marie Skłodowska-Curie grant agreement number 675746 (PROFILE) and from the Netherlands Ministry of Health (PPOC-18-022).

Disclosure of Conflicts

B.E., N.A.G.G., and J.V. are inventors on a patent application regarding autoantibody-resistant ADAMTS13 variants.

References

1. Kremer Hovinga JA, Coppo P, Lammle B, et al. Thrombotic thrombocytopenic purpura. *Nat. Rev.* 2017;3:1–17.
2. Hrdinova J, Dangelo S, Graca A.G. N, et al. Dissecting the pathophysiology of immune thrombotic thrombocytopenic purpura. *Haematologica* 2018;103(7):1099 -1109.
3. Joly BS, Coppo P, Veyradier A. An update on pathogenesis and diagnosis of thrombotic thrombocytopenic purpura. *Expert Rev. Hematol.* 2019;12(6):383–395.
4. Pos W, Crawley JTB, Fijnheer R, et al. An autoantibody epitope comprising residues R660, Y661, and Y665 in the ADAMTS13 spacer domain identifies a binding site for the A2 domain of VWF. *Blood*. 2010;115(8):1640–1649.
5. Pos W, Luken BM, Kremer Hovinga JA, et al. VH1-69 germline encoded antibodies directed towards ADAMTS13 in patients with acquired thrombotic thrombocytopenic purpura. *J. Thromb. Haemost.* 2009;7(3):421–428.
6. Thomas MR, de Groot R, Scully MA, Crawley JTB. Pathogenicity of Anti-ADAMTS13 Autoantibodies in Acquired Thrombotic Thrombocytopenic Purpura. *EBioMedicine*. 2015;2:942–952.
7. Pos W, Sorvillo N, Fijnheer R, et al. Residues Arg568 and Phe592 contribute to an antigenic surface for anti-Adamts13 antibodies in the spacer domain. *Haematologica*. 2011;96(11):1670–1677.
8. Jian C, Xiao J, Gong L, et al. Gain-of-function ADAMTS13 variants that are resistant to autoantibodies against ADAMTS13 in patients with acquired thrombotic thrombocytopenic purpura. *Blood*. 2012;119(16):3836–3843.
9. Ercig B, Wichapong K, Reutelingsperger CPM, et al. Insights into 3D Structure of ADAMTS13 : A Stepping Stone towards Novel Therapeutic Treatment of Thrombotic Thrombocytopenic Purpura. *Thromb. Haemost.* 2018;28–41.
10. Graca N A.G., Ercig B, Velasquez Pereira LC, et al. Modifying ADAMTS13 to modulate binding of pathogenic autoantibodies of patients with acquired thrombotic thrombocytopenic purpura. *Haematologica*. 2019;105(11):2619-2630.
11. Luken BM, Kaijen PHP, Turenhout EAM, et al. Multiple B-cell clones producing antibodies directed to the spacer and disintegrin/thrombospondin type-1 repeat 1 (TSP1) of ADAMTS13 in a patient with acquired thrombotic thrombocytopenic purpura. *J. Thromb. Haemost.* 2006;4(11):2355–2364.
12. Weitzner BD, Jeliazkov JR, Lyskov S, et al. Modeling and docking antibody structures with Rosetta. *Nat. Protoc.* 2017;12:401–416.
13. Leem J, Dunbar J, Georges G, Shi J, Deane CM. ABodyBuilder: Automated antibody structure prediction with data–driven accuracy estimation. *MAbs*. 2016;8(7):1259–1268.
14. Akiyama M, Takeda S, Kokame K, Takagi J, Miyata T. Crystal structures of the noncatalytic domains of ADAMTS13 reveal multiple discontinuous exosites for von Willebrand factor. *Proc. Natl. Acad. Sci. U. S. A.* 2009;106(46):19274–19279.
15. Van Zundert GCP, Rodrigues JPGLM, Trellet M, et al. The HADDOCK2.2 Web Server: User-Friendly Integrative Modeling of Biomolecular Complexes. *J. Mol. Biol.* 2016;428(4):720–725.

16. Case DA, Cerutti DS, Cheatham III TE, Darden TA, Duke RE, Giese TJ, Gohlke H, Goetz AW, Greene D, Homeyer N, Izadi S, Kovalenko A, Lee TS, LeGrand S, Li P, Lin C, Liu J, Luchko T, Luo R, Mermelstein D, Merz KM, Monard G, Nguyen H, Omelyan I, Onufriev A, Pan F, Qi R, Roe DR, Roitberg A, Sagui C, Simmerling CL, Botello-Smith WM, Swails J, Walker RC, Wang J, Wolf RM, Wu X, Xiao L, York DM, Kollman PA, 2017, AMBER 2017, University of California, San Francisco.
17. Miller BR, McGee TD, Swails JM, et al. MMPBSA.py: An efficient program for end-state free energy calculations. *J. Chem. Theory Comput.* 2012;8(9):3314–3321.
18. Wichapong K, Alard J-E, Ortega-Gomez A, et al. Structure-Based Design of Peptidic Inhibitors of the Interaction between CC Chemokine Ligand 5 (CCL5) and Human Neutrophil Peptides 1 (HNP1). *J. Med. Chem.* 2016;59(9):4289–4301.
19. Wichapong K, Poelman H, Ercig B, Hrdinova J. Rational modulator design by exploitation of protein – protein complex structures. *Future Med. Chem.* 2019;11(9):1015–1033.
20. Kokame K, Nobe Y, Kokubo Y, Okayama A, Miyata T. FRETS-VWF73, a first fluorogenic substrate for ADAMTS13 assay. *Br. J. Haematol.* 2005;129(1):93–100.

Supplementary Data

Supplemental information

Structural bioinformatics pipeline to build antigen-autoantibody complexes

RosettaAntibody module[1] and ABodyBuilder[2] were used to model the Fv fragments of II-1 and I-9 autoantibodies.[3,4] The framework regions (FRs) and complimentary determining regions (CDRs) were detected automatically and were built based on homology. Heavy chain CDR3 loop (CDR-H3) was modelled by the ab-initio modeling module which is implemented in RosettaAntibody. Sphinx[5], a method that combines ab-initio and knowledge-based methods was employed to model CDR-H3 loops for the autoantibody models which were prepared by ABodyBuilder. 3D models of autoantibodies II-1 and I-9 were docked onto the spacer domain epitope (Protein Data Bank: 3GHM) using HADDOCK.[6] The docking procedure was driven by ambiguous interaction restraints between the known epitope region on spacer domain (R568/F592/R660/Y661/Y665) and (CDR-H3) of II-1 and I-9 autoantibodies. All docking poses generated by HADDOCK were further duplicated into a second set, in which gain-of function (GoF) ADAMTS13 mutations (R568K/F592Y/R660K/Y661F/Y665F)[7] were introduced using PyMOL 1.8.2.1 (The PyMOL Molecular Graphics System, Version 1.8.2.1 Schrödinger, LLC).

Both wild type (WT)- and GoF-spacer-autoantibody complexes were prepared for subsequent molecular dynamics (MD) simulations using AMBER16 and AmberTools16, assigning the FF14SB forcefield.[8] TIP3P[9] water model was used to solvate the system within a 10 Å radius of the molecular surface of the spacer-autoantibody complex. The total charge of the system was neutralized by random exchange of water molecules with sufficient amounts of Na^+ or Cl^- ions. The position of the solvent molecules with the fixed solute molecule were adjusted by steepest descent energy minimization through 2000 steps which was followed by 2000 steps of conjugate gradient algorithm. An additional energy minimization for the entire system was next applied without any restraints on the solvent and the solute. After convergence reached in energy minimization, the system was heated from 0 to 300 K, using position-restrained MD simulation in which the solute molecule was restrained with weak force constant (10 kcal/mol•A^2), up to 100 ps with 1ps^{-1} collision frequency on Langevin dynamics. Next, the system was equilibrated for 400 ps using the same restraining parameters at constant temperature (300 K). After reaching an equilibration in the system, a restraint-free, production MD simulation was performed for 100 ns for each system at a constant temperature (300K) and pressure (1 bar). In every step (2 fs) of the entire MD simulation, SHAKE algorithm[10] was applied to maintain the correct bond geometry. Electrostatic and non-bonded interactions were calculated by Particle-mesh Ewald (PME)[11] at a 10 Å cutoff.

MMPBSA.py[12] was employed to calculate the binding free energy (BFE) between

the spacer domain and the autoantibodies. In this study, the BFE difference between WT- and GoF-ADAMTS13 against autoantibodies was used as a selection criterion. As shown in the literature[7] and here, autoantibodies II-1 and I-9[3,4] targeting the major epitope in spacer domain bind to WT-ADAMTS13, whereas they do not bind to GoF-ADAMTS13.[7] As described in several studies, use of MD snapshots following the energy minimization steps or short MD simulations can be utilized for relative BFE calculation .[13,14] Thus, to accelerate our calculations, after each interval of 10 ns MD simulation, each WT-pose with a lower BFE comparing to its GoF-pose was kept, otherwise was discarded. The BFE calculation was calculated using the following formula:

$$\Delta G^{o}_{bind,solv}=\Delta G^{o}_{bind,vacuum}+\Delta G^{o}_{solv,complex}-(\Delta G^{o}_{solv,ligand}+\Delta G^{o}_{solv,receptor})$$

$$\Delta G_{bind,aq} = \Delta H - T\Delta S \approx \Delta_{EMM}+\Delta G_{bind,solv} - T\Delta S \quad (1)$$

$$\Delta_{EMM}=\Delta_{Ecovalent}+\Delta_{Eelectrostatic}+\Delta_{EvdW} \quad (2)$$

The sum of van der Waals, electrostatic interaction, internal energy and solvation energy equals to the enthalpy (ΔH). Solvation energy was calculated by solving generalized Born (GB) model 8. BFEs were calculated at every 100th step of 10 ns interval (a frame per 0.01 ns interval) on each MD simulation trajectories. The entropy term (-TΔS) was ignored for each system in BFE calculation, since the entropy calculations do not significantly improve the trend of the relative BFE of similar complexes and also they are computationally expensive to calculate.[15,16] The energy decomposition per residue was calculated after each 10 ns interval of the MD simulation, in order to obtain a better understanding of the interactions at atomic level which provided a further insight on exploring a larger epitope landscape on ADAMTS13 spacer domain.

Recombinant ADAMTS13 production and mutation insertions

The wild type gene of human ADAMTS13 was cloned into mammalian expression vector pQMCF3 (Icosagen Cell Factory, Estonia) and transiently expressed in a CHO cell line cultivated in a chemically defined medium (BalanCD CHO Transfectory, Irvine Scientific, USA) supplemented with 6 mM Glutamax and 1% Penicillin/Streptomycin (GibCo, USA). Mutations in the spacer exosite-3 were inserted by means of synthetic oligonucleotides of the region of interest flanked by *Xma*I (540bp) or *Acc*I (360bp; both native cloning sites of ADAMTS13 WT gene) and *Hind*III (artificially inserted by silent mutation of residues Q684 and A685 resulting in an overall change of 5”-CAGGCCT-3’ to 5’-C<u>AAGCTT</u>-3’; Genewiz, Leipzig, Germany). A larger oligonucleotide (1245bp) of the ADAMTS13 WT gene (spanning from F494 to C908, covering the cysteine-rich domain to the TSP1-repeat 5 domain) flanked by the native *Pag*I and *Esp3*I cloning sites, and also containing the same native cloning sites mentioned above as well as an artificially introduced *XhoI* site (silent mutation of the nucleotide sequence encoding L621, resulting in an overall change from 5’-CTGGAG-3’ to 5’-<u>CTCGAG</u>-3’) which

was inserted into a pUC57 vector (Genewiz, Leipzig, Germany). This plasmid was used to exchange the WT sequence by the smaller synthetic DNA fragments carrying the mutations of interest by means of *Xma*I/*Hind*III or AccI/*Hind*III. The complete ADAMTS13 1245 bp fragments were then used to replace this section of the WT sequence of ADAMTS13 in the pQMCF3 vector through *Pag*I/*Esp*3I. All constructs were sequenced before transfection. The DNA was transfected to a CHO cell line according to published protocol.[17] At 24 h post transfection, fresh medium was added in 50% of culture volume, and a temperature shift from 37°C to 30°C was made when cells achieved density > 3 x 10^6 mL^{-1}. Feed 4 (Irvine Scientific) was added at 0.6% concentration in 6% of culture volume every two days, and cultures monitored for viability using the trypan blue exclusion method. Culture media were collected when viability dropped below 90% and serine protease inhibitor phenylmethylsulfonyl fluoride (PMSF) was added (0.5 mM). Protein production was confirmed by western blotting using either a mouse anti-His-tag (1:2500; GenScript, USA) and goat anti-mouse IgG-HRP (1:8000; Invitrogen), or an anti-V5-HRP (1:5000; Invitrogen). The recombinant ADAMTS13 concentration was measured as previously explained. [18,19]

Supplementary table 1. List of generated full-length ADAMTS13 mutants.

Mutation	Original sequence	Mutated sequence
L591A	P**L**$_{591}$FTH	P**A**$_{591}$FTH
K608A	G**K**$_{608}$MSI	G**A**$_{608}$MSI
M609A	K**M**$_{609}$SIS	K**A**$_{609}$SIS
R636A	D**R**$_{636}$LPR	D**A**$_{636}$LPR
L637A	R**L**$_{637}$PRL	R**A**$_{637}$PRL
L668A	N**L**$_{668}$TRP	N**A**$_{668}$TRP
NGLY1	A**R**$_{568}$**EY**$_{570}$V	A**N**$_{568}$**ET**$_{570}$V
NGLY2	P**L**$_{591}$**FT**$_{593}$H	P**N**$_{591}$**FT**$_{593}$H
NGLY3	G**K**$_{608}$**MS**$_{610}$I	G**N**$_{608}$**MS**$_{610}$I
NGLY4	K**M**$_{609}$**SI**$_{611}$S	K**N**$_{609}$**SS**$_{611}$S
NGLY5	D**R**$_{636}$**LP**$_{638}$R	D**N**$_{636}$**LS**$_{638}$R
NGLY6	R**L**$_{637}$**PR**$_{639}$L	R**N**$_{637}$**AS**$_{639}$L

Measuring the binding of patient anti-ADAMTS13 autoantibodies to ADAMTS13 variants

The wells of Nunc MaxiSorp flat-bottom 96-well plates (ThermoFisher Scientific) were coated with 100 ng monoclonal antibody 3H9 overnight. After coating, wells were blocked with 2% BSA in phosphate buffered saline (PBS). Wells were then incubated with 200ng of ADAMTS13 or MDTCS. Subsequently, patient-derived monoclonal autoantibodies II-1 (9.3ng/ml) and I-9 (111.1 ng/ml) or 100 µl of diluted patient's samples were tested with each ADAMTS13 variants. Any patient derived autoantibodies

which were bound to ADAMTS13 were incubated with 100µl of a mixture of anti-human IgG1, IgG2, IgG3 and IgG4 monoclonal antibodies, conjugated with horseradish peroxidase and diluted in 1:10000 (Sanquin, The Netherlands). Reactivity of autoantibodies from each patient serum with ADAMTS13 variants was compared to the reactivity observed for WT-ADAMTS13. Reactivities of patient sera against all ADAMTS13 variants were expressed as a percentage of the binding in a heatmap format which was created by Graphpad Prism 8.

FRETS-VWF73 activity assay for ADAMTS13 variants

Diluted culture media containing the ADAMTS13 NGLY variants at a concentration of 1.05 nM (0.2 µg/ml) were used for these assays. ADAMTS13 was first diluted in an activity buffer composed of 20 mM HEPES, 20 mM Bis-Tris, 20 mM Tris-HCl, 25 mM $CaCl_2$ (pH 6.0) supplemented with 0.005% Tween20 to 2.10 nM in a 100 µl volume. Then, the reaction was started by adding FRETS-VWF73 substrate (100 µl, 4 µM), diluting further ADAMTS13 to 1.05 nM. In parallel, a calibration curve was generated in a similar manner using the WT ADAMTS13 diluted in a concentration range of 0.13125–2.10 nM. The activity-levels of the ADAMTS13 variants were calculated and compared to that of WT ADAMTS13 with final concentration of 1.05 nM, which was set at 100%. The activity measurements in the presence of patient sera was determined as described above, before addition of the FRETS-VWF73 substrate, the ADAMTS13 variants (2.10 nM) were each incubated in the presence of 10 µl of patient sample or PBS for 30 mins at 37 °C. The final volume was 210 µl of which 10 µl belonged to the added patient plasma or PBS (for control). Activity-levels of wild-type ADAMTS13 1.05 nM incubated in the absence of patient sample were set at 100%.

VWF multimer assay for measuring the activity of ADAMTS13 variants

To measure the ability of different ADAMTS13 variants to process VWF multimers 0.2 µg of each ADAMTS13 variant was incubated for 30 mins at 37°C in an activation buffer composed of 20 mM Bis-Tris, 20 mM Tris-HCl, 20 mM HEPES, 25 mM CaCl2 (pH 7.5), 0.005% Tween20 and supplemented with 2% Bovine Serum Albumin fraction V (Merck) (ADAMTS13 = 3.8 nM). In parallel, human recombinant VWF produced in HEK293 cells was incubated with 3 M urea for 30 min at 37°C at a final concentration of 80 nM. Denatured recombinant VWF multimers were then added to the ADAMTS13 containing mixture at a 1 to 1 ratio (final ADAMTS13=1.9 nM; final VWF=40 nM). The capacity of the different ADAMTS13 variants to cleave VWF in these conditions is visualized by the disappearance of High-Molecular Weight (HMW) multimers from the top of the gel, and accumulation of cleavage products seen through higher intensity of bands in the lower part of the gel, as well as the appearance of satellite bands. Samples were collected and quenched with 4x loading buffer (composition: urea

9.6 M, 4% SDS m/v, Tris-base 0.035 M, EDTA 25 mM, Bromophenol blue 7.5 μM, no pH adjustment) at 0 and 30 minutes and 24 hours to assess the ability of the different ADAMTS13-NGLY1-6 variants to process VWF.

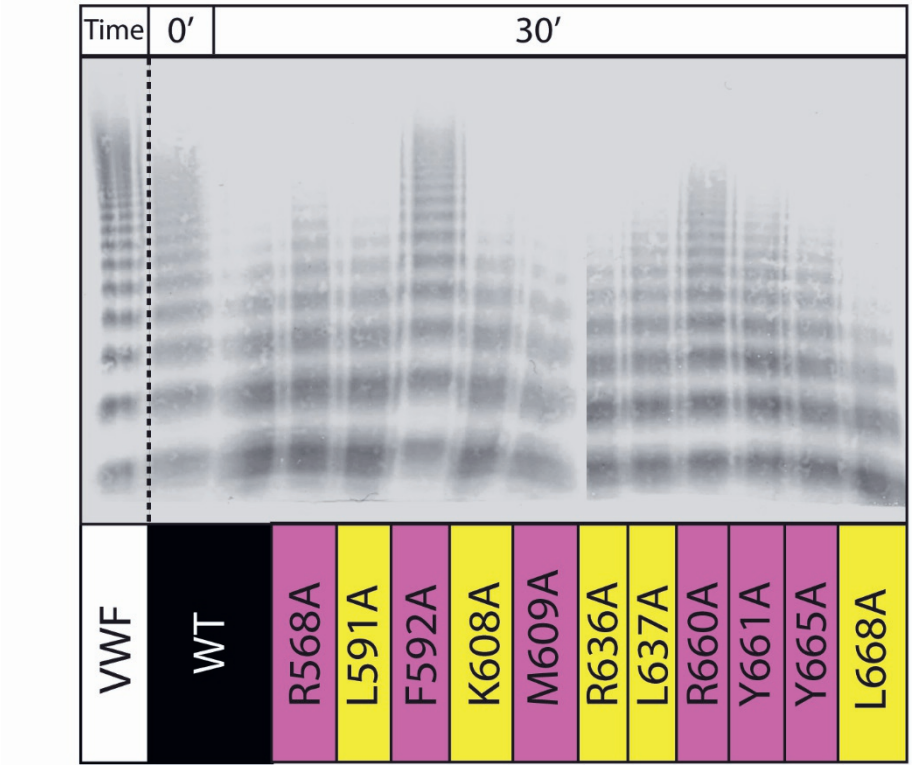

Supplementary figure 1 – VWF multimer assay for testing the proteolytic activity of single alanine mutants of ADAMTS13.

Mass Spectrometry based identification of N-glycan modified ADAMTS13

WT-ADAMTS13, NGLY3 and K608A variants were purified from expression medium by immunoprecipitation using anti-V5 antibody coupled to magnetic beads (Dynabeads M-280 Sheep Anti-Mouse IgG) at room temperature for 1 hour. The magnetic beads were washed three times with an ice-cold buffer containing 10 mM Tris-HCl (Thermo Scientific), 150 mM NaCl(Thermo Scientific), 0.5 mM EDTA. Rapid PNGase F (New England Biolabs) was used to trim the N-glycans of ADAMTS13 on magnetic beads, according to guidelines of the manufacturer, at 37°C, overnight. The deglycosylation of ADAMTS13 was confirmed by observing a molecular weight loss in western blot using anti-V5 conjugated to a horseradish peroxidase (data not shown).

The same wash buffer was used on the magnetic beads to wash away PNGase F and the reaction buffer. Both PNGase F treated and untreated samples were reduced on-beads with 1 M urea(Sigma), 100 mM Tris-HCl pH7.5, 10 mM DTT(Thermo Scientific) followed by alkylation with 50 mM iodoacetamide (Thermo Scientific). Bound ADAMTS13 was detached from the beads using 250 ng Trypsin Gold (Promega), followed by incubation overnight at 25°C to generate tryptic peptides. Samples were loaded on In-house prepared C18 stage tips (EMPORE 3M) and the desalted and concentrated peptides were eluted using 80 % acetonitrile (BioSolve), 0,5% acetic acid (Sigma). Samples were speed-vacuum dried and resuspended in 2% acetonitrile, 0.1% trifluoroacetic acid (Thermo Scientific) followed by LC-MS analysis using an Orbitrap Fusion (Thermo Scientific). The RAW mass spectrometry files were processed with Proteome Discoverer 2.2 (Thermo Scientific). Proteins and peptides were identified using the Sequest HT search engine by querying the human Uniprot database (downloaded February 2019) and a database containing the mutant ADAMTS13 sequences. Settings used were 10 ppm tolerance for the precursor mass and 0.6 Da tolerance for fragment masses. Oxidation (M) and deamidation (N) were set as dynamic modifications, carbamydomethylation (C) as static modification. Only peptides with high confidence (FDR < 0.05) were used for protein identification.

The presence of a N-glycan at NGLY3-ADAMTS13 was investigated by peptide coverage in mass spectrometry by the detection of K608N deamidation upon deglycosylation. PNGaseF mediated deglycosylation reaction removes the entire N-glycan structure from an asparagine, which deamidates the side chain and converts the asparagine into an aspartic acid. As expected, in the non-PNGaseF treated NGLY3-ADAMTS13, the peptide containing the putative N-glycan at K608N was not detected. However, when the same sample was treated with PNGaseF, the peptide (residues between 603-629) was found to have a deamidated asparagine (at position 608) converted into an aspartic acid residue. Both WT- and K608A ADAMTS13 were used as controls to further provide confidence to our assay for the events which occurred were specific for the presence of an N-glycan. Different peptide coverage profiles were observed due to the mutations at K608 and trypsin cleavage between WT, NGLY3 and K608A-ADAMTS13. Only non-PNGaseF treated WT-ADAMTS13 sample provided a peptide-of-interest (residues 599-608). Both non-PNGaseF treated NGLY3 and K608A-ADAMTS13 did not present any peptide of interest due to mutation of trypsin cleavage site at K608 and presence of a native N-glycan at position 614. However, all PNGaseF treated samples of WT, NGLY3 and K608A-ADAMTS13 samples were found a have deamidation of asparagine to aspartic acid at position 614 due to the presence of a native N-glycan, as expected.

Supplementary References

1. Weitzner BD, Jeliazkov JR, Lyskov S, et al. Modeling and docking antibody structures with Rosetta. *Nat. Protoc.* 2017;12:401–416.
2. Leem J, Dunbar J, Georges G, Shi J, Deane CM. ABodyBuilder: Automated antibody structure prediction with data–driven accuracy estimation. *MAbs*. 2016;8(7):1259–1268.
3. Luken BM, Kaijen PHP, Turenhout EAM, et al. Multiple B-cell clones producing antibodies directed to the spacer and disintegrin/thrombospondin type-1 repeat 1 (TSP1) of ADAMTS13 in a patient with acquired thrombotic thrombocytopenic purpura. *J. Thromb. Haemost.* 2006;4(11):2355–2364.
4. Pos W, Luken BM, Kremer Hovinga JA, et al. VH1-69 germline encoded antibodies directed towards ADAMTS13 in patients with acquired thrombotic thrombocytopenic purpura. *J. Thromb. Haemost.* 2009;7(3):421–428.
5. Marks C, Nowak J, Klostermann S, et al. Sphinx: Merging knowledge-based and ab initio approaches to improve protein loop prediction. *Bioinformatics*. 2017;33(9):1346–1353.
6. Van Zundert GCP, Rodrigues JPGLM, Trellet M, et al. The HADDOCK2.2 Web Server: User-Friendly Integrative Modeling of Biomolecular Complexes. *J. Mol. Biol.* 2016;428(4):720–725.
7. Jian C, Xiao J, Gong L, et al. Gain-of-function ADAMTS13 variants that are resistant to autoantibodies against ADAMTS13 in patients with acquired thrombotic thrombocytopenic purpura. *Blood*. 2012;119(16):3836–3843.
8. Maier JA, Martinez C, Kasavajhala K, et al. ff14SB: Improving the Accuracy of Protein Side Chain and Backbone Parameters from ff99SB. *J. Chem. Theory Comput.* 2015;11(8):3696–3713.
9. Jorgensen WL, Chandrasekhar J, Madura JD, Impey RW, Klein ML. Comparison of simple potential functions for simulating liquid water. *J. Chem. Phys.* 1983;79(2):926–935.
10. Ryckaert JP, Ciccotti G, Berendsen HJC. Numerical integration of the cartesian equations of motion of a system with constraints: molecular dynamics of n-alkanes. *J. Comput. Phys.* 1977;23(3):327–341.
11. Darden T, York D, Pedersen L. Particle mesh Ewald: An $N \cdot \log(N)$ method for Ewald sums in large systems. *J. Chem. Phys.* 1993;98(12):10089–10092.
12. Miller BR, McGee TD, Swails JM, et al. MMPBSA.py: An efficient program for end-state free energy calculations. *J. Chem. Theory Comput.* 2012;8(9):3314–3321.
13. Rastelli G, Rio A Del, Degliesposti G, Sgobba M. Fast and accurate predictions of binding free energies using MM-PBSA and MM-GBSA. *J. Comput. Chem.* 2009;31(4):797–810.
14. Wichapong K, Lawson M, Pianwanit S, Kokpol S, Sippl W. Postprocessing of protein-ligand docking poses using linear response MM-PB/SA: Application to Wee1 kinase inhibitors. *J. Chem. Inf. Model.* 2010;50(9):1574–1588.
15. Wichapong K, Alard J-E, Ortega-Gomez A, et al. Structure-Based Design of Peptidic Inhibitors of the Interaction between CC Chemokine Ligand 5 (CCL5) and Human Neutrophil Peptides 1 (HNP1). *J. Med. Chem.* 2016;59(9):4289–4301.
16. Uciechowska U, Schemies J, Scharfe M, et al. Binding free energy calculations and biological testing of novel thiobarbiturates as inhibitors of the human NAD+ dependent histone deacetylase Sirt2. *Medchemcomm*. 2012;3(2):167.

17. Karro K, Männik T, Männik A, Ustav M. Chapter 29: DNA Transfer into Animal Cells Using Stearylated CPP Based Transfection Reagent. *Springer*; 2015.
18. Graca N A.G. Ercig B, Velasquez Pereira LC, et al. Modifying ADAMTS13 to modulate binding of pathogenic autoantibodies of patients with acquired thrombotic thrombocytopenic purpura. *Haematologica*. 2019;105(11):2619-2630.
19. Dekimpe C, Roose E, Tersteeg C, et al. Anti-ADAMTS13 autoantibodies in immune-mediated thrombotic thrombocytopenic purpura do not hamper ELISA-based quantification of ADAMTS13 antigen. *J. Thromb. Haemost.* 2020;18:985–990.